A study on the properties of fractal electronic quantum systems

(Supervised by Stephen R. Power)

Juan J. Vazquez,* Aleksander Prymek,† Octavian Stoicescu,‡ and Stephen R. Power
School of Physics, Trinity College Dublin, Dublin 2, Ireland

Recent developments in technology allow us to control matter on the nano-scales. This enabled the creation and study of electronic quantum systems (EQS). Artificial atomic lattices allow for more precise and complex systems to be realised in experiments, which includes non-integer/fractal systems. In this project, we have computationally modelled and analysed the electronic properties of a system with the geometry of three variations of the Sierpinski triangles fractal using Python.

I. INTRODUCTION AND THEORY

The creation and study of electronic quantum systems (EQS) is a very active field in condensed matter physics and materials science. Artificial atomic lattices allow for more precise and complex systems to be realised in experiments due to the larger length scales involved. It is possible to obtain EQS which have previously only been considered theoretically or to reproduce and manipulate unusual behaviour from graphene using instead molecules on metallic surfaces.

The electronic structure of such systems can be described using a simple tight-binding Hamiltonian

$$H = \sum_i \epsilon_i c_i^\dagger c_i - \sum_{\langle i,j \rangle} t_{ij}(c_i^\dagger c_j + H.c), \qquad (1)$$

where the on-site energy is denoted by ϵ, t_{ij} is the hopping term between sites i and j, $H.c$ is the Hermitian conjugate and $c_i^\dagger$ and c_j are the creation and annihilation operators.

The properties displayed by an EQS, particularly the emergence of localisation in defected systems, are highly dependent on dimensionality. Artificial lattices allow such studies to be easily extended to systems with non-integer dimensions, that is, fractal EQS, which were the goal of this project.

Several studies [1, 2] have already investigated experimentally the electronic properties of systems equipped with fractal geometries. The fractal lattice investigated in those experiments and in this project - the Sierpinski triangles lattice - has a Hausdorff dimension of 1.58.

In [1], a Sierpinski triangle fractal lattice was experimentally engineered. A clean Cu(111) crystal surface was set up, and a scanning tunneling microscope (STM) was used to position CO molecules by lateral manipulation, forming a triangle of the same size as a $G(3)$ Sierpinski fractal lattice. Then lateral manipulation was used again to remove the redundant molecules from the triangle thus forming a $G(3)$ fractal - the desired geometry.

The aim of our project was to computationally model and analyse similar geometries. We have studied three different variations of the Sierpinski fractal lattice which are shown below in the Fig. 1.

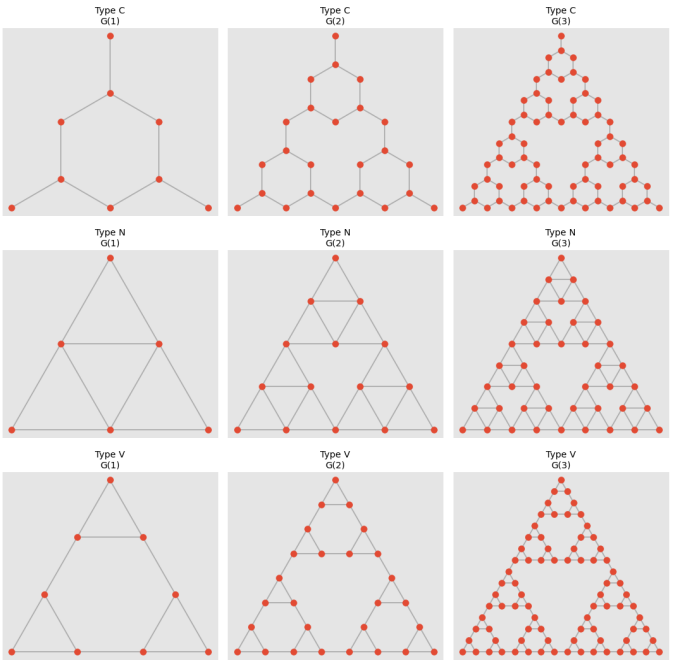

FIG. 1. The first three iterations of the three variations of the Sierpinski triangle fractal lattices that were studied. The type N lattice was obtained by removing the centre points of each unit triangle in the type C lattice. The type V lattice was obtained by separating the vertices of each unit triangle in the type N lattice such that the unit triangles do not share vertices.

A. Green's Function and Density of States

Formally, a Green's function (GF) is a solution of a linear differential equation with a Dirac delta inhomogeneous source with homogeneous boundary conditions. It is a potent tool often used for solving quantum mechanical problems, since the conception of Quantum Mechanics in the early 20th century as it is possible to rewrite the Schrodinger equation, where normally one would solve

* vazquezj@tcd.ie
† prymeka@tcd.ie
‡ stoicesco@tcd.ie

for wave functions, in terms of the Green's function. For more detail refer to [3].

The Hamiltonian in the Eq. (1) can be written in the matrix representation as

$$H = H_0 + V = \sum_a |\Psi_a\rangle \, \epsilon_a \, \langle\Psi_a| + V, \tag{2}$$

where V is the operator representing the interactions between the sites. It is mostly zero, $V_{ij} = 0$, except when the sites i and j are the nearest-neighbours (for simplicity only the nearest-neighbour hopping is considered in this project), then $V_{ij} = t$.

This allows us to find the GF in the matrix representation which is defined as

$$g = \lim_{\eta \to 0} \left[(E \pm i\eta) I - H_0 \right]^{-1}, \tag{3}$$

where $\pm$ gives us a choice between the advanced GF $(+)$ and retarded GF $(-)$.

If we substitute for H_0 in the above, we get

$$g = \lim_{\eta \to 0} \sum_a |\Psi_a\rangle \, \frac{1}{E + i\eta - \epsilon_a} \, \langle\Psi_a| \, . \tag{4}$$

Assuming an LCAO-type Hamiltonian, we can describe H_0 by a basis of localised orbitals $|j\rangle$, centred on site j. Projecting onto orbitals $|j\rangle$ and $|l\rangle$ gives

$$g_{jl} \equiv \langle j| \, g \, |l\rangle = \lim_{\eta \to 0} \sum_a \langle j|\Psi_a\rangle \, \frac{1}{E + i\eta - \epsilon_a} \, \langle\Psi_a|l\rangle \tag{5}$$

$$= \lim_{\eta \to 0} \sum_a \langle j|\Psi_a\rangle \, \frac{E - i\eta - \epsilon_a}{(E - \epsilon_a)^2 + \eta^2} \, \langle\Psi_a|l\rangle \, . \tag{6}$$

Taking the imaginary part, then setting $j = l$ and using the following definition of the Dirac Delta function

$$\delta(x) = \frac{1}{\pi} \lim_{a \to 0} \frac{a}{x^2 + a^2}, \tag{7}$$

allows us to write

$$-\frac{1}{\pi} \operatorname{Im}(g_{jj}) = \sum_a |\, \langle j|\Psi_a\rangle \,|^2 \delta(E - \epsilon_a). \tag{8}$$

Which is the definition of the Local Density of States (LDOS) at site j. Hence, we have a way of finding the density of states from the GF.

B. Recursive Green's Function

Finding the Hamiltonian for any system is straightforward. However, for complex systems, the Hamiltonian matrix is very large, and so inverting it (which is necessary to find the GF) is timely and computationally expensive. Instead of using brute force (matrix inversion), we can use a recursive method.

Consider two systems: the 'clean'/initial system defined by $H = H_0$, $g = (EI - H_0)^{-1}$ and the perturbed system defined by $H = H_0 + V$, $G = [EI - (H_0 + V)]^{-1}$. Then, we can write

$$\begin{aligned} G^{-1} = (EI - H_0) - V = g^{-1} - V \\ \implies G^{-1}G = g^{-1}G - VG \\ \implies g = gg^{-1}G - gVG \\ \implies G = g + gVG. \end{aligned} \tag{9}$$

Eq. (9) is called the Dyson equation. It allows us to find the GF of a complex, perturbed system from the GF of simpler 'clean' system without the need for inverting large matrices.

II. METHODOLOGY

A. Slicing the Lattice

To find the GF of the whole Sierpinski lattice recursively we divide it into cells such that each consecutive cell contains only the nearest-neighbours of the previous cell. Hence, before slicing the lattice we need to decide which sites should the first cell contain. To calculate the transport properties of the lattice we need to know the G matrix values corresponding to the sites that connect to leads. In fact, it is enough to know those values alone as the values of the G are not localised like that of the Hamiltonian (changing a value of ϵ_i affects only a single entry of the Hamiltonian, H_{ii}; but when it comes to the GF, all entries are affected which follows from the fact that G is found by inverting H). Hence, we should choose the first cell such that the last cell will contain the points joining to the leads (in our case those are any two vertices). Alternatively, as realised in the project, we can choose the first cell to have the desired points, and after slicing the lattice reverse the order of cells.

B. Finding the Green's Function Recursively

Consider a system consisting of only the first N cells. Take G^M_{ij} to be the GF between the cells i and j after the Mth cell has been added, g_{ii} to be the GF of the disconnected ith cell, and $V_{N,N+1}$, $V_{N+1,N}$ to be the matrices connecting the $(N+1)$st cell and Nth cell.

If we just want the GF of the last cell, it follows that

$$G^{N+1}_{N+1,N+1} = \frac{g_{N+1,N+1}}{1 - g_{N+1,N+1} V_{N+1,N} G^N_{N,N} V_{N,N+1}}. \tag{10}$$

This identity holds only if each cell is connected to those cells that are 'before' and 'after' it so that only $V_{N\pm1,N}$ and $V_{N,N\pm1}$ are non-zero.

C. Finding DOS Recursively

As shown in the Eq. (8) we can find the DOS from the GF. Hence, it is possible to find the DOS recursively.

The DOS after adding the $(N+1)$st cell is

$$D^{N+1} = -\frac{1}{\pi}\,\mathrm{Im}\sum_{i=1}^{N+1}\mathrm{Tr}(G_{i,i}^{N+1}). \tag{11}$$

For $0 \le i \le N$ we have

$$G_{i,i}^{N+1} = g_{i,i}^{N} + g_{i,N}^{N} V_{N,N+1} G_{N+1,N+1}^{N+1} V_{N+1,N} g_{N,i}^{N}. \tag{12}$$

Thus,

$$\begin{aligned} D^{N+1} = -\frac{1}{\pi}\,\mathrm{Im}\Bigg\{ & \sum_{i=1}^{N}\mathrm{Tr}\left(g_{i,i}^{N}\right) \\ & + \mathrm{Tr}\left[G_{N+1,N+1}^{N+1} V_{N+1,N}\left(\sum_{i=1}^{N} g_{N,i}^{N} g_{i,N}^{N}\right) V_{N,N+1}\right] \\ & + \mathrm{Tr}\left(G_{N+1,N+1}^{N+1}\right)\Bigg\} \qquad (13) \\ = D^{N} & - \frac{1}{\pi}\,\mathrm{Tr}\left[G_{N+1,N+1}^{N+1}(A_{N+1}+I)\right], \qquad (14) \end{aligned}$$

where

$$\begin{aligned} A_{N+1} &= V_{N+1,N}\left(\sum_{i=1}^{N} g_{N,i}^{N} g_{i,N}^{N}\right) V_{N,N+1} \qquad (15) \\ &= V_{N+1,N} g_{N,N}^{N}(A_N + I) g_{N,N}^{N} V_{N,N+1}. \qquad (16) \end{aligned}$$

D. Conductance

To model the conductance two semi-infinite leads were connected to two vertices of the lattice. The conductance through the system is given, in terms of GFs, by

$$G = G_0 T_{LR}, \quad \text{where} \quad T_{LR} = \mathrm{Tr}(\Gamma_L G_R \Gamma_R G_A). \tag{17}$$

$\Gamma_{L/R} = i\left(\Sigma_R - \Sigma_A\right)$ is a broadening matrix (related to self energy which captures the effect of adding the left-/right lead to the device), G_R and G_A are the retarded and advanced GFs. G_0 is the conductance quantum, i.e. the quantized unit of electrical conductance defined in terms of the elementary charge e and Planck constant h:

$$G_0 = \frac{2e^2}{h} \approx 7.748\,091\,729 \times 10^{-5}\,\mathrm{S}. \tag{18}$$

E. Modelling

The lattices were modelled using Python language. The equations (10), (14), (16) and (17) were programmed in order to find all the quantities needed recursively.

The comparison of the execution time between the brute force inversion method and the recursion method was made.

Additionally, an option was added to change the on-site energy of some sites to simulate impurities/defects in the lattice. Change of the on-site energy corresponds to inserting an atom of a different element. Also, the eigenstates were plotted and Inverse Participation Ratio (IPR) was calculated for both pristine and defected lattices to show the localisation of states in the defected systems.

III. RESULTS AND CONCLUSIONS

A. Execution Time

First, the number of points for a lattice of first five iterations was plotted (Fig. 2) to show that the complexity of the system increases exponentially as lattices of higher and higher iteration are modelled.

From the Fig. 2 we can expect that the brute force method may be faster for the small systems (low iteration lattices), but relatively quickly it will be too expensive to run. Its biggest challenge will be the memory allocation as large chunks of memory will be needed to invert matrices with couple thousand or couple million entries, especially since Python is a high level language.

And indeed, as we can see in the Fig. 3, the inversion method is faster for first four iterations, but for iterations five and above the recursive method becomes significantly more efficient. Also, when running the brute force method for iteration six on a modern laptop `MemoryError` occurred. Clearly, the recursive method is more efficient and less expensive for simulating this and any complex EQS that can be divided into cells.

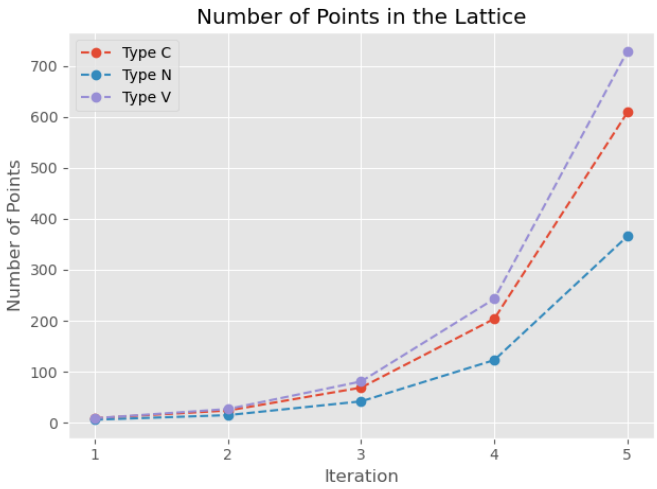

FIG. 2. The number of points/sites in the lattice for the first five iterations.

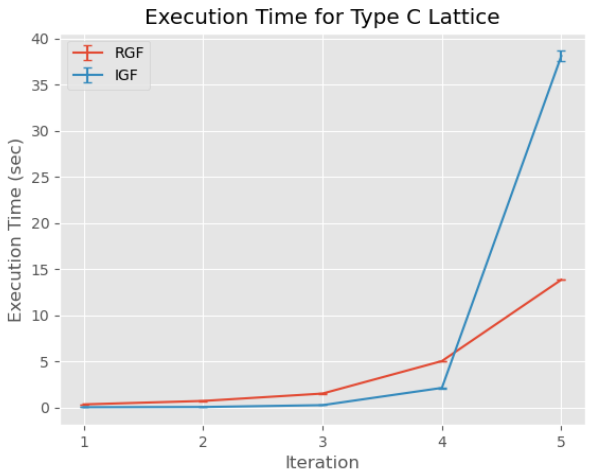

FIG. 3. The graph of the time necessary for each method to calculate values of the GF and DOS for 1,000 energy values for the first five iterations of the type C lattice.

B. Eigenstates and DOS of Defective Lattices

Defects have been added to the lattices and their properties were compared to those of the pristine lattices (figures are included in the Appendix).

The defects were implemented by randomly selecting sites and changing the on-site energy ϵ to significantly higher values compared to the non-defected sites. This type of impurities corresponds to replacing the atom with an atom of a different element.

Another method of adding impurities would be to change the hopping term to and from a defective site. This in turn would correspond to a change in potential at the site caused, for example, by adsorption of a molecule/atom to the lattice. Unfortunately, due to time constraints, this type of defect was not explored in the project.

Visually comparing the allocation of the same eigenstates in the impure and pristine lattices (Fig. 4, 5 and 6), it is easy to see that the impure lattices tend to have highly localised eigenstates. This was also shown by plotting the IPR of both pristine and impure lattices (Fig. 7).

The following values were used for all plots: $\eta = 0.001$, $t = -1$, $\epsilon_{\text{normal}} = 0$, $\epsilon_{\text{defect}} = 100$, fraction of defected sites= 20%. The 'first' eigenstate was plotted, however, eigenvalues are not necessarily ordered in any way as `numpy.linalg.eig` was used to compute them. S

C. Transport

Due to the time constraints, the DOS was not analysed in depth.

An expected property of a fractal lattice would be the self-similarity of the DOS, however, our model does not seem to produce results confirming this phenomenon. In fact, the DOS of the type N and V lattices tends to be asymmetrical around 0 energy, which was not anticipated and could not have been explained by the authors suggesting an error in the model.

Another point of concern was negative values of DOS obtained after the leads were connected to the lattice which is a standard step in analysing the transport properties of a system. To avoid the negative values, the absolute values of the DOS were plotted in the Fig. 8 instead. The Fig. 8 also contains plots of the conductance as a function of energy. As expected, the plots of conductance bears some similarity with the plots of DOS.

[1] S. N. Kempkes, M. R. Slot, S. E. Freeney, S. J. M. Zevenhuizen, D. Vanmaekelbergh, I. Swart, and C. M. Smith, Nature Physics **15**, 127–131 (2018).
[2] S. N. Kempkes, M. R. Slot, J. J. V. D. Broeke, P. Capiod, W. A. Benalcazar, D. Vanmaekelbergh, D. Bercioux, I. Swart, and C. M. Smith, Nature Materials **18**, 1292–1297 (2019).
[3] M. M. Odashima, B. G. Prado, and E. Vernek, Revista Brasileira de Ensino de Física **39**, 10.1590/1806-9126-rbef-2016-0087 (2016).
[4] L. Yan and P. Liljeroth, Advances in Physics: X **4**, 1651672 (2019).

IV. APPENDIX

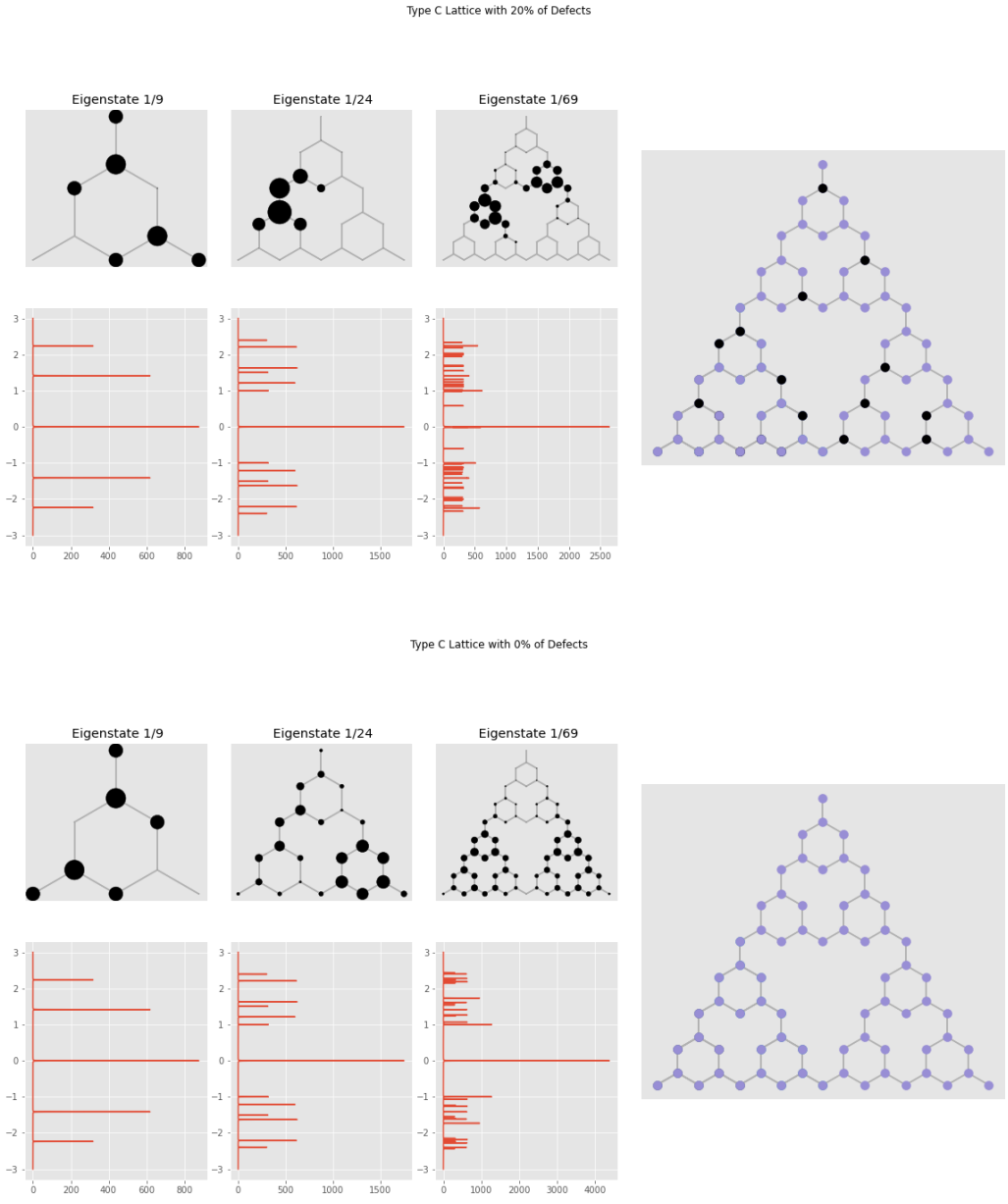

FIG. 4. The spatial distribution of eigenstates and DOS of the defected (top) and pristine (bottom) type C lattices for its first three iterations. The leftmost graph shows the third iteration of the lattice with defective sites in black.

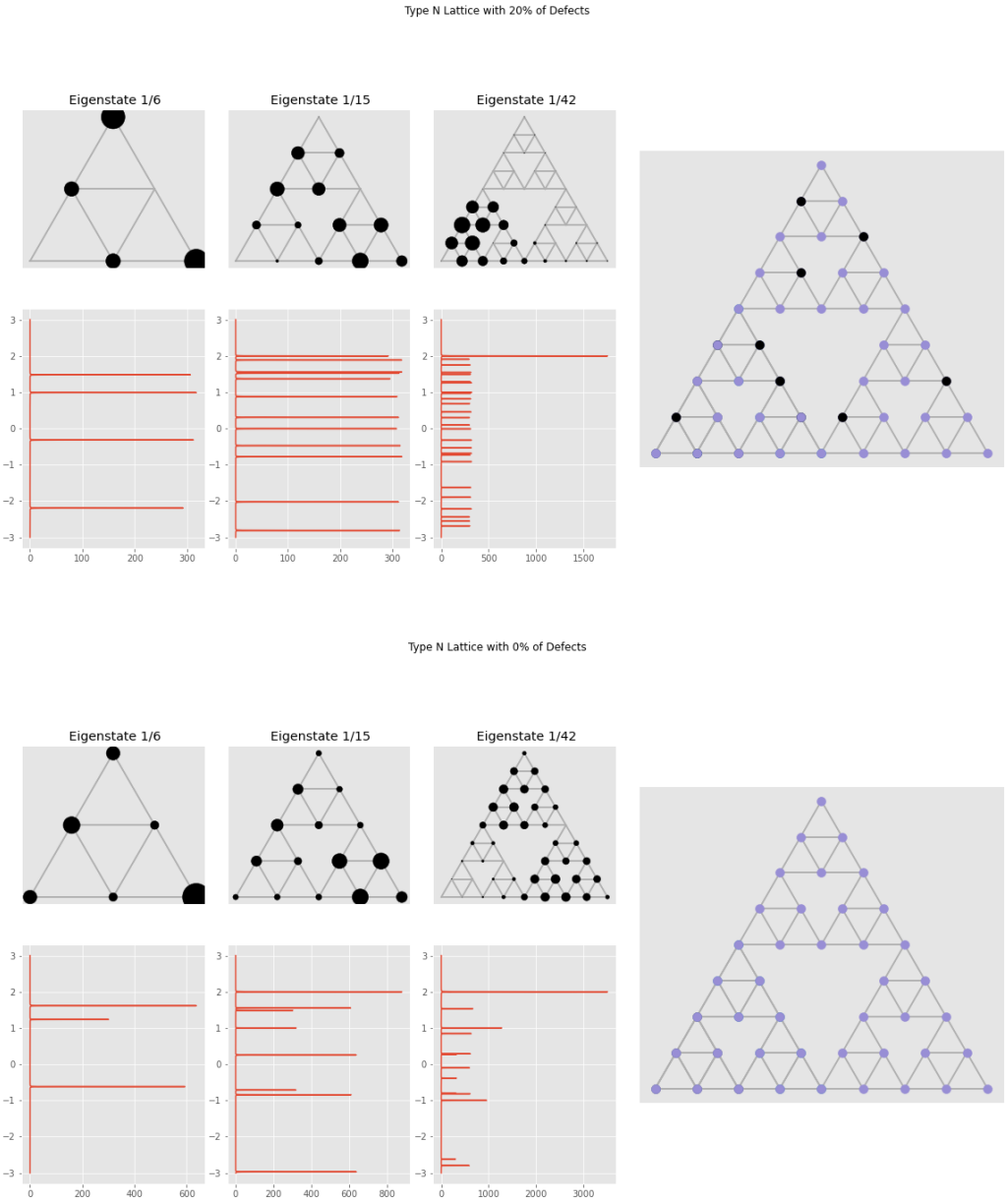

FIG. 5. The spatial distribution of eigenstates and DOS of the defected (top) and pristine (bottom) type N lattices for its first three iterations. The leftmost graph shows the third iteration of the lattice with defective sites in black.

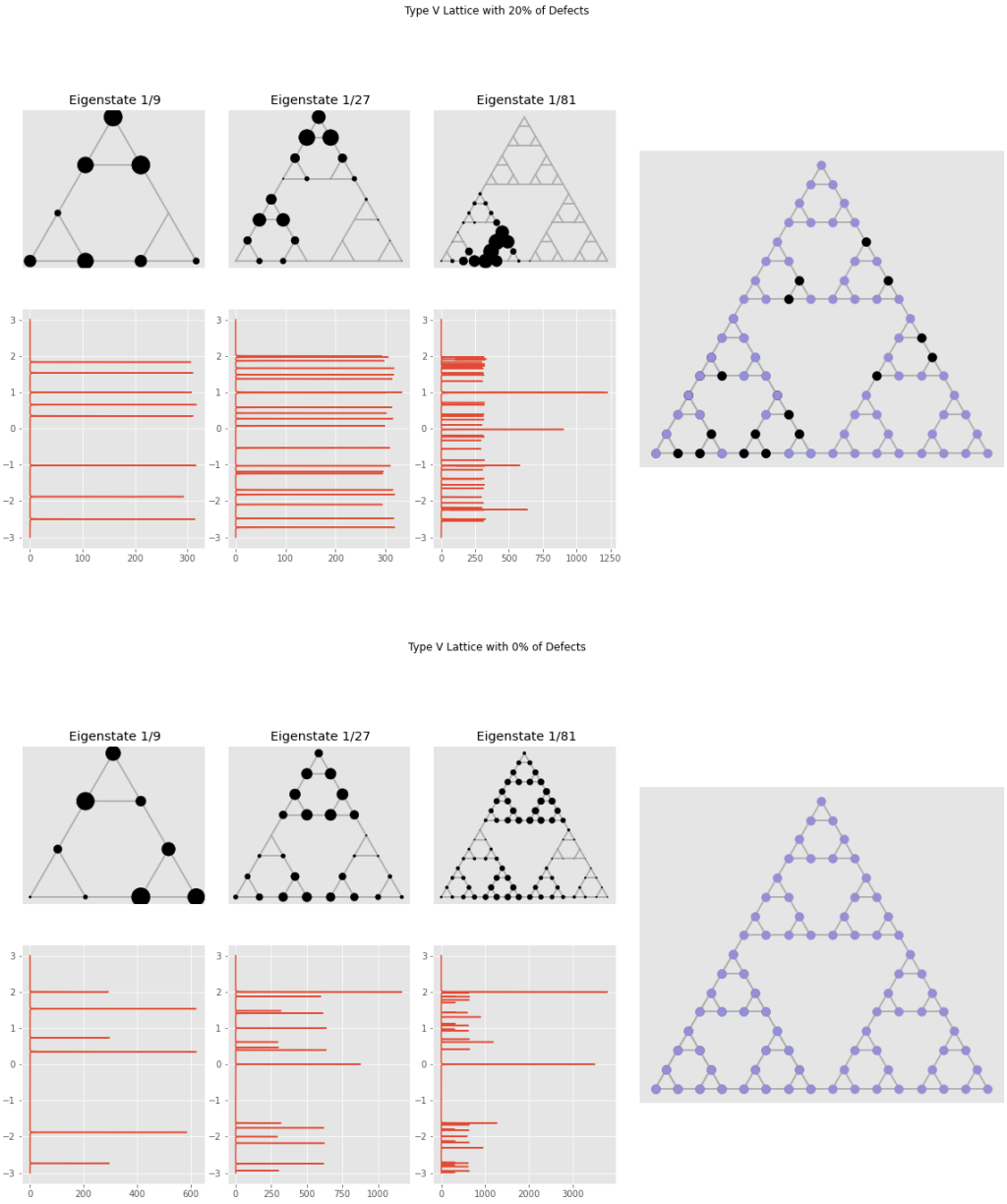

FIG. 6. The spatial distribution of eigenstates and DOS of the defected (top) and pristine (bottom) type V lattices for its first three iterations. The leftmost graph shows the third iteration of the lattice with defective sites in black.

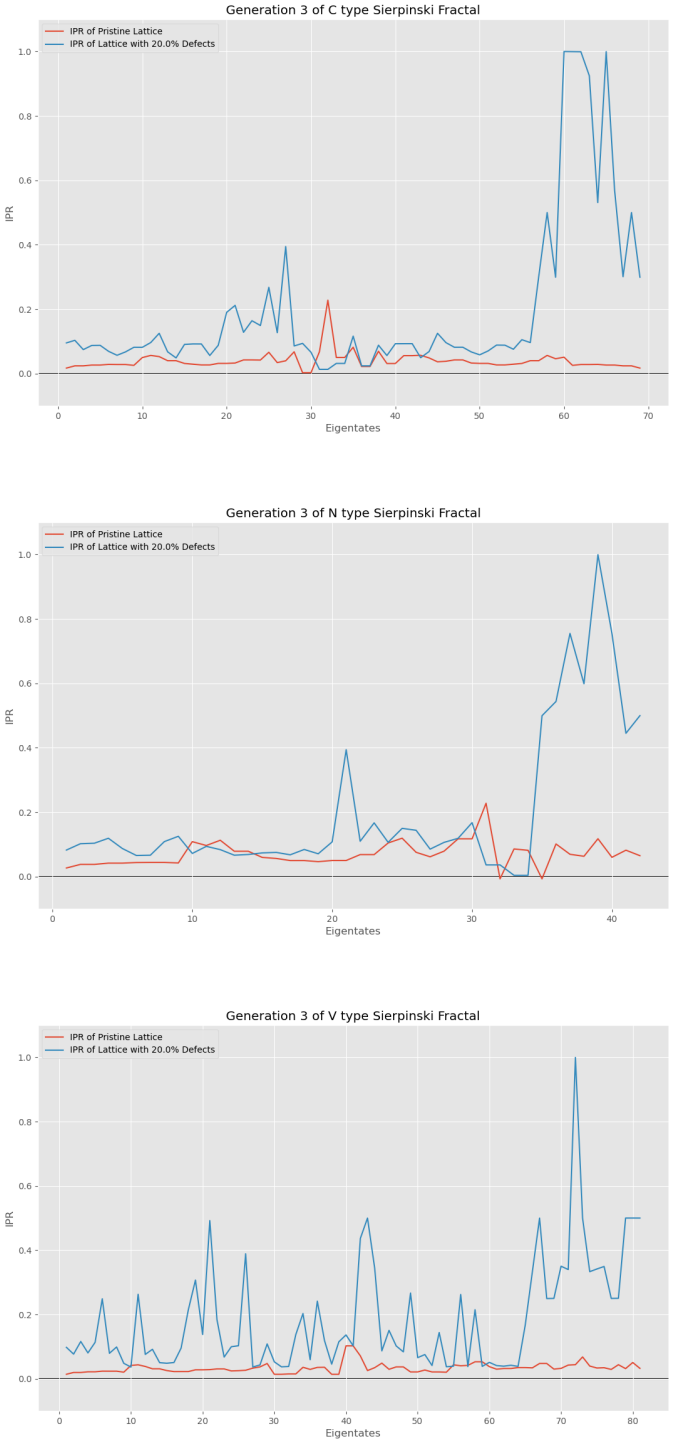

FIG. 7. The IPR for both pristine and impure third-generation lattices. For the majority of states, the IPR of the defected lattices is greater, showing the emergence of localisation in defected systems.

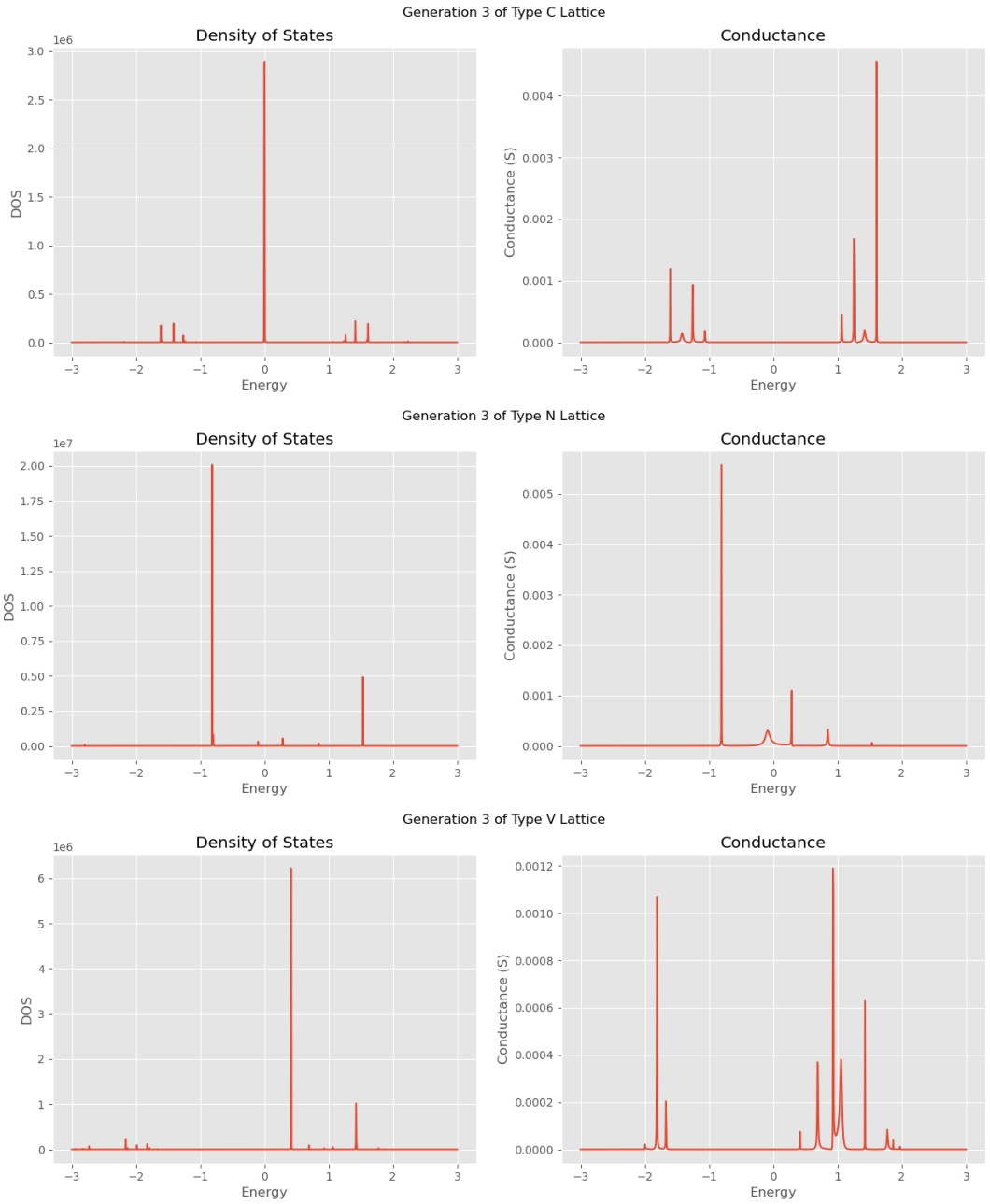

FIG. 8. The DOS and conductance of the pristine third-generation lattices.